Geoelectrical Characterization of Sulphate Rocks

Ander Guinea Maysounave

Programa de Doctorat de Ciències de la Terra

GEOELECTRICAL CHARACTERIZATION OF SULPHATE ROCKS

Ander Guinea Maysounave

2011

Advisors / Directors de tesi:

Drs. Elisabet Playà Pous & Lluís Rivero Marginedas

Departament de Geoquímica, Petrologia i Prospecció Geològica

UNIVERSITAT DE BARCELONA

Annex 3

Journal of Applied Geophysics (2012)

Ander Guinea 2011

THE ELECTRICAL PROPERTIES OF CALCIUM SULPHATE ROCKS FROM DECAMETRIC TO MICROMETRIC SCALE

Ander Guinea[1]*, Elisabet Playà[1], Lluís Rivero[1], Juan José Ledo[2], Pilar Queralt[2]

[1]*Departament de Geoquímica, Petrologia i Prospecció Geològica. Facultat de Geologia, Universitat de Barcelona (UB). Martí i Franquès s/n, 08028 Barcelona, Spain.*

[2]*Departament de Geodinàmica i Geofísica. Facultat de Geologia, Universitat de Barcelona (UB). Martí i Franquès s/n, 08028 Barcelona, Spain.*

E-mails: anderguinea@ub.edu; eplaya@ub.edu; lrivero@ub.edu; jledo@ub.edu; pilar.queralt@ub.edu

*Corresponding author: *Phone number: +34 934 03 11 65. Fax number: +34 934 02 14 17*

ABSTRACT

Sulphate rocks have a sedimentary evaporitic origin and are present in many deposits worldwide. Among them, gypsum (dihydrated calcium sulphate) is the most common and it is exploited with industrial purposes. Anhydrite (calcium sulphate) is frequently found in gypsum quarries and in no-outcropping sulphates. Because of its higher hardness comparing with gypsum, it suppose a problem for the extraction of gypsum; the fronts of the quarries in which anhydrite is found are stopped at the moment when it appears. The electrical properties of calcium sulphates have been studied by means of geoelectrical methods. The conductivity of gypsum crystals has been tested in different crystalographical directions showing that the plane (010) in which the water molecules are aligned is more conductive. The lack of this structure in the crystals of anhydrite explains its larger electrical resistivity.

A direct relationship between the electrical conductivity values of the calcium sulphate rocks and their lithological composition has been established being the lutitic matrix the main controlling factor when it is percolant (connected at long range). When the matrix is under the percolation threshold the dominant phases are the sulphate ones and the electrical response of the rocks depends on the percentage of each one in their composition. When the rock is

matrix dominant, the electrical resistivity trend fits with the Hashin-Shtrikman lower bound for multiphase systems (considering gypsum, anhydrite and matrix as the components). On the other hand, when the rock is calcium sulphate dominant the trend shows the one of the Hashin-Shtrikman upper bound. The reference electrical resistivity value of pure anhydrite rocks has been defined as 104 ohm.m and geoelectrical classification for calcium sulphate rocks has been elaborated. With this classification it is possible to differentiate between calcium sulphate rocks with different composition from their electrical resistivity value. This classification has been checked with field examples and calculating the theoretical resistivity value of thin section photographs with the program ELECFEM2D. The electrical behavior of calcium sulphate rocks is a good reference for other type of rocks with electrically differentiated components, and similar methods can be used to define their geoelectrical responses.

Keywords: Gypsum, Anhydrite, Sulphate, Electrical Conductivity

1. INTRODUCTION

Evaporites are sedimentary rocks originated from evaporitic processes, this is, have been precipitated from water following the evaporative concentration of dissolved salts. Sulphates are one of the principal groups of evaporitic rocks and the principal sulphate minerals are: gypsum (CaSO4·2H2O), anhydrite (CaSO4), glauberite (Na2Ca(SO4)2) and thenardite (Na2SO4) among others. Texturally, sulphate rocks are mainly crystalline; even they also can appear with clastic textures when they are reworked. They retain only reduced primary porosity (<1%), display a restricted mineralogical (and geochemical) composition and can appear combined and/or with a lutitic (mainly composed of clay and microcrystalline carbonates) matrix. These rocks are extensively affected by diagenetic processes which can change their texture into microcrystalline. Gypsum tends to transform into anhydrite when buried because of dehydration and the opposite process also takes place when anhydrite is affected by weathering and superficial waters.

Gypsum deposits are exploited with industrial purposes. It is mainly used in construction as drywall and ingredient for plaster but it is also used in other industries.

Gypsum quarries are developed worldwide with USA and Iran as the first producing countries. One of the most important problems found while quarrying gypsum is the presence of anhydrite. Comparing with gypsum, anhydrite has different physical properties as higher hardness and density. The drilling machines can be damaged because of this hardness and when an anhydrite body appears, the exploitation must be stopped immediately. Anhydrite is also used in industry for different purposes, but because of the exploitation difficulties it is mainly obtained from dehydration of previously extracted gypsum. Anhydrite (coming from gypsum dehydration) is commonly found at deeply buried units (>500 m, in general), it rarely outcrops because it tends to hydrate and transform into gypsum.

As a tool for studying these sulphate deposits, geoelectrical techniques are proposed. Electrical resistivity tomography (ERT) is a geophysical technique which obtains an image of the electrical resistivity distribution of the subsurface. On this purpose a string of iron electrodes are disposed on the surface of the terrain and the difference of electrical potential is measured between two of them while a direct current (DC) is injected by other two ones. The arranging of these 4 electrodes depends on the selected electrical array and the measure is repeated along the string of electrodes at different spacing and positions. The obtained apparent resistivity values are inverted into real resistivity ones with an inversion software. ERT is a rapid, non invasive and relatively low-cost method.

Gypsum deposits have been successfully identified with ERT profiles (Lugo et al., 2008; Guinea et al., 2009; Guinea et al., 2010a). Guinea et al. (2010b) elaborated a geoelectrical classification of gypsum rocks establishing a direct relation between its electrical resistivity value and the percentage of lutitic matrix (table 1). In that study the anhydrite phase was not considered, but this mineral very often appears in gypsum rocks. Respecting anhydrite rocks published geoelectrical surveys show a large range of resistivity value from <100 to 1010 omh.m (table 2). The variation in the electrical resistivity value of anhydrite in these publications is related to the presence of gypsum, but the influence of the lutitic matrix is not mentioned. The aim of this study is to define the electrical resistivity of pure anhydrite and establish the effect of compositional variations in the gypsum-anhydrite-lutite rock system. This problem will be studied from three different angles, namely numerical modeling, laboratory measurements and field data. Obtained information would help to interpret geoelectrical data in the future surveys on sulphate rocks and to interpret electrical resistivity value of other rock groups formed of various components with different electrical properties.

2. FIELD DATA

2.1 Methods

A total of nine ERT profiles have been performed upon anhydrite rock deposit areas in the South Pyrenean Foredeep and Ebro Basin (North East of Spain; Figure 1). The examples are presented below starting with the ones performed in quarries (figure 1, A, B, C, D, E, F and G) and afterwards in areas with no-outcropping evaporites (figure 1, H and I). All the profiles performed in quarries show high purity of sulphates and therefore relatively high electrical resistivity values.

A Syscal Pro Switch with 48 electrodes and external power supply has been used to carry out the data acquisition. The electrode spacing for the measures in quarries has been 1, 1.5 or 2 meter depending on the logistical availability. In the profiles performed in no-outcropping evaporite zones the electrode spacing selected has been 10m to increase the investigation depth because anhydrite deposits tend to be under sedimentary basins (otherwise they transform into gypsum; even this process also can take place at depth). There are many possible array configurations in geophysical prospection (Ma et al., 1997; Furman et al., 2003; Szalai and Szarka, 2008) for measuring anhydrite rocks, Wenner-Schlumberger and Dipole-Dipole have been selected depending of the structure under study (Dipole-Dipole has been used in the case of dominating lateral electrical resistivity changes). The apparent resistivity data of performed ERT profiles has been inverted with RES2DINV program. The code consists in the algorithm of smoothness-constrained least squares (deGroot-Hedlin and Constable, 1990; Sasaki 1992; Loke and Barker, 1996). The inversion process has been carried out with 5 iterations for each profile. With this number of iterations the data converges in all cases achieving an acceptable RMS error; additional iterations do not vary significantly the RMS error but increase the electrical resistivity value in the low sensitivity areas (this is, the pure sulphate rocks). As it is explained later on section 2.3, the values obtained for inverted electrical resistivity data (with 5 iterations) in expected pure anhydrite bodies are likely to those of apparent ones measured directly on observed anhydrite rocks.

Complementary to the ERT surveys, sulphate samples have been collected in some of the studied areas in order to measure the amount of matrix on them. The samples have been powdered and 0.5g from each one has been dissolved in 250 ml of distilled water in accordance with the solubility in water of calcium sulphate. The solutions have been shaken during 24 hours and filtered afterwards. The residue left after filtering correspond with the

non-soluble phases, this is, the lutitic matrix (including carbonates, quartz and other minor accompaining minerals), which can be weightened and quantified in order to estimate the purity in sulphate phases of the calcium sulphate deposits.

2.2 Geological settings

During the Lutetian (Middle Eocene) a large marine evaporitic sequence was deposited in the South Pyrenean Foredeep (Rosell and Pueyo, 1997). In La Garrotxa area (eastern Pyrenees) secondary gypsum (as product of the hydration of anhydrite) outcrops extensively and anhydrite has been found in borehole logs with other evaporitic rocks as halite (Carrillo, 2009). Close to the village of Beuda (Girona, Spain) there is a quarry in which gypsum is exploited since at least the decade of 1930. There are many sculptures made of alabaster (pure secondary microcrystalline gypsum) from the middle age in which geochemical analysis has demonstrated that they were extracted from the Beuda gypsum unit (Inglés et al., 2009).

Nowadays the quarry has been largely developed (figure 2A) and anhydrite outcrops in many places in which the exploitation has been stopped because of its presence. The gypsum of Beuda unit came from the hydration of anhydrite and therefore there are still some anhydrite relicted bodies embedded in the gypsum. In the walls of the quarry it is possible to observe boundaries between gypsum and anhydrite usually displaying a quite pure anhydrite core and a transition to pure gypsum (figure 2B). The purity of the calcium sulphates vary from higher than 90% to close to 75% in certain layers (figure 2C). The changes in the purity of both gypsum and anhydrite rocks and the complex geometrical relations between them make these deposits very heterogeneous. In some cases matrix bearing gypsum appears in contact with pure anhydrite (figure 2D) and in other cases the anhydrite does not appear as a body but as fragments embedded in gypsum and filled with gypsum veins (figure 2E). In other places anhydrite appears massive with little gypsum within (figure 2F). Five ERT profiles (figure 3, A, B, C, D and E) have been performed in Beuda gypsum quarry. The profile H (figure 3H) has been performed in the same formation of the quarry of Beuda, close to the village of Serinyà. In the area studied there are sulphate layers under a cropping field. In the nearby outcrops pure secondary gypsum appears, but in depth, the sulphates would transform into anhydrite as it has been observed in the region (Carrillo, 2009).

Marine evaporitic deposition took place during the upper Eocene in the Catalan margin of Ebro basin (Ayora et al., 1994). The Odena gypsum unit was extensively exploited during the XXth century and the region is plenty of abandoned quarries. The profiles F and G have been

performed in abandoned quarries near to the village of Odena where anhydrite outcrops (figure 2G).

In the Montes de Torrero area (Zaragoza, Spain) there is a Miocene evaporitic formation hundreds of meters thick. During the construction of the Spanish high velocity train (AVE) railways the area was studied by mean of boreholes in which gypsum, anhydrite, glauberite and halite were found among other minerals. This formation has a large quantity of matrix in every layer (Ortí, 2000; Salvany, 2009). The outcropping materials are mainly gypsum coming from the hydration of anhydrite or glauberite (figure 2H) and with more than 50% of matrix (composed of clay and marl). An ERT survey has been performed where the borehole B4 was drilled (figure 3I). The log of the borehole shows gypsum until 35 meter depth and below glauberite until 69 meter depth and anhydrite until 80 meter depth with some interbedded layers of halite or glauberite (Salvany, 2009). The whole log has important quantity of matrix as it is seen in the surface.

2.3 Results and discussion

In the quarry of Beuda some different areas have been studied. The profiles A, B and C have been performed upon areas in which massive anhydrite was found and afterwards was buried under quarry waste materials. The profiles were spread above the infilling. The result of the inversion for the profiles A and B (figure 3, A, B) display an upper part with relatively low electrical resistivity values (between 10 and 200 ohm.m) which would correspond to the quarry waste. Underlying these materials there is a homogeneous body with high resistivity value (up to 104 ohm.m) interpreted as pure anhydrite. In the case of profile C, it was performed perpendicularly to profile B. The inverted resistivity section (figure 3C) displays a lateral electrical resistivity variation below the quarry waste layer. With a drilling machine the center part was drilled (no log was recovered) and at 6 meter depth high hardness was found. This hardness has been interpreted as anhydrite rock with certain quantity of impurities.

Profiles D and E have been measured in other places in which anhydrite had stopped the exploitation of the quarry. The electrodes were nailed almost directly on the sulphate rocks and both anhydrite and gypsum appeared in the ground surface. In both inverted resistivity sections (figure 3, D and E) there is displayed a lateral variation of electrical resistivity ranging from 103 to 104 ohm.m. The larger resistivity values are bounded to the outcropping of massive anhydrite while the lower ones are related to the presence of gypsum; the intermediate values correspond to the transition of both sulphate phases. In the profile E

the inversion calculate a very resistive body (more than 3x104ohm.m) which probably corresponds to a cavity, usual in sulphate rocks.

The profiles F and G have been performed in abandoned quarries near to the village of Odena where anhydrite outcrops (figure 2G). The inverted section shows electrical resistivity ranging from 103 to 104 ohm.m; similarly to what has been observed in the quarry of Beuda (Figures 3F and G). In the areas in which the value is larger massive anhydrite is observed. Lower electrical resistivity than 500 ohm.m are related to lutitic sedimentary layers.

The profiles H and I have been performed in no-outcropping evaporitical basins. The inversion of the profile H (figure 3H) displays a shallow deposit with low electrical resistivity value (50 ohm.m) which corresponds with the underlying materials. Below this layer there is a high resistivity body ranging from 1000 to more than 5000 ohm.m and with a more conductive structure in the center part (between 100 and 200 ohm.m). This structure represents a fault present in the area and identified in surface with geological evidences (Carrillo, 2009). The profile I performed in Montes de Torrero area has been modified from Guinea et al. (2010b). In the inverted image (figure 3I) the whole deposit shows a general trend of 30-50 ohm.m with some bodies slightly more resistive (until 300 ohm.m in the most resistive point). Those bodies would represent a higher purity of the deposit (up to 60% in purity in sulphates) in these zones, this purity changes are related to primary depositional processes and they are very common in these materials (Guinea et al., 2010a). In any case it is not possible to differentiate between anhydrite and gypsum layers because the electrical behavior of the deposit is dominated by the abundant matrix.

As general trend, sulphate rocks with high purity in anhydrite show an electrical resistivity value up to 104 ohm.m after the inversion. This value is considered to be the reference for pure anhydrite rocks because in some profiles in which some of the shallowest points have been measured almost directly above massive anhydrite rocks, show an apparent resistivity value larger than 5000 ohm.m. In these cases the apparent and the inverted resistivities are similar but a little bit lower for the apparent one because the electrodes are nailed on a thin clay layer. When these rocks are mixed with gypsum forming pure sulphate rocks with both phases, which are the most common ones in the quarries, they display an intermediate value of resistivity ranging from 1500 to 5000 ohm.m depending the quantity of each phase. As the distribution of the anhydrite in the gypsum deposits is very heterogeneous due to the rehydration processes, the tomography lines show heterogeneous bodies with

different electrical resistivity values and transitional zones. Values close to 1000 ohm.m are related to the purest gypsum rocks or to pure anhydrite with a significant quantity of matrix rocks. When the presence of matrix is large, there is no possibility of differencing gypsum from anhydrite with ERT. The low electrical resistivity value of sulphate deposits with less than 60% in purity was studied further by Guinea et al. (2010b) for the case of gypsum rocks (without anhydrite).

3. LABORATORY ESSAYS

3.1 Methods

Several authors have performed conductivity measuring tests for geological materials (Keller, 1966; Daily et al., 1995; Ewanic et al., 2001; Giao et al., 2003; Vanhala et al., 2009; Rusell and Barker, 2010; among others). Guinea et al (2010b) elaborated eleven gypsum-clay pills in different proportions (at intervals of 10% composition ranges from 0 to 100% in $CaSO4{\cdot}H2O$) and measured their electrical conductivity. Following the same methodology, parameters and resources, eleven anhydrite-lutite pills have been elaborated. Additionally, the 4 purest pills prepared by Guinea et al. (with purity in gypsum ranging from 70 to 100%) have been repeated in order to be measured again with more accurateness using a nanoammeter instead of the microammeter used formerly. The aim of these measures is to define the importance of the matrix presence in calcium sulphate rocks.

In addition, 12 pure monocrystal gypsum sheets have been elaborated in order to observe possible electrical conductivity differences. Anhydrite crystal sheets have not been elaborated due to the difficulty of obtaining a crystal large enough as to perform such essay. The electrical conductivity of different mineral crystals has been already measured previously by many authors (Telkes, 1950; Bleaney and Bleaney, 1976; Keller, 1966; Tomioka et al., 1998; Halpern, 1998; Zou et al., 2009; among others). From the sheets, 6 have been cut parallel and 6 cut perpendicular to the main exfoliation planes. The gypsum crystals tend to break along these exfoliation planes so in order to cut the sheets perpendicularly to this structure; the crystal has been previously embedded within a non conductive poliester resin (Norsodyne ref.9944). The thickness of crystal samples has been measured with a vernier caliper.

The measure of conductivity has been carried out in accordance with the UNE 21-303-33 regulation (1983) with an electrical circuit in which the samples act as electrical resistance (figure 4A). The electrical power source was a laboratory DC converter power supply with switchable voltage (0–32 V) and amperage (0-10 A). Changes in the amperage above 1A do not affect the essays so output amperage of 2A has been selected. In order to measure the amperage of the electrical current after traversing the resistance (the sample), a microammenter or a nanoammeter (Monroe, mod. 285) with a range of ±200 nA and 0.1 nA resolution and an accuracy of 2% have been used. In the case of crystal sheets, the electrodes have been elaborated sticking insulating tape defining a rectangular tape-free surface in which an electrically conductive gel (Compex gel for ultrasonic transmission and electrostimulation) has been poured; spreading along the surface of the electrode. The two poles of the circuit cable are connected to the gel in both sides of the samples by foil grasped to copper clamps (figure 4B). The electrical current run by the gel surface and crosses the sample perpendicularly to it. This is due to the fact of that the current tends to seek the most conductive way to spread, and the opposite gel electrode is the most conductive body towards which be directed; so the lateral leakages can be despised. The rock brick and the electrode assemblage are situated above a paperboard insulator in order to prevent possible leakages. The measures have been taken switching on the power supply and waiting few seconds until the reading stabilizes (10 seconds); after a time the sample start to be polarized and the reading tend to increase. The longest time measures are not considered representatives for geophysical surveys because geoelectrical methods use a short current injection time. Ohm's law can be applied to calculate the conductivity (σ) or resistivity (ρ) of the sample for a known current density (j) and field (E) (Eq. 1):

Equation 1:
$$j = \sigma E = E/\rho$$

It is possible to measure the resistance (R) of the samples. As the thickness (L) of the sample and the surface area of the electrode (S) are known, the electrical resistivity (ρ) can be calculated in another form of the Ohm's law (Eq. 2):

Equation 2:
$$R = \rho \, {}^{L}/_{S}$$

The laboratory essays in crystal sheets have been carried out 5 times and the average value has been selected as the representative one. The selected voltage is 1V for exfoliation

parallel cut sheets and 0.1V for exfoliation perpendicularly cut sheets. The selection of 1V in the case of samples parallel to the exfoliation planes is due to that there is no reading with 0.1V. The size of the electrode and the width of the sheet depend on the limitations of each crystal. Crystal sheets with impurities have been discarded to avoid conducting channels not related to the crystalline structure. An electrical resistivity test has been previously performed on the resin (0.3cm-thick resin sample with a 6cm2 electrode, at 32.2 V) to prove its not conductive nature.

3.2 Results and discussion

The new measures performed in anhydrite-lutite pills have shown a similar trend to the one presented by Guinea et al. (2010b) for a gypsum-lutite pill set. The pills ranging from 0 to 50% in anhydrite purity (Pa1 to Pa6; table 3) display a very scarce increasing trend of the electrical resistivity value (from 6 to 21 ohm.m). The pills ranged from 80 to 100% in anhydrite purity (Pa9 to Pa11; table 3) where out of scale of the microammeter and therefore they were measured with the nanoammeter showing higher electrical resistivity values (from 1870 to 13457 ohm.m). The 60 and 70% anhydrite purity pills (Pa7 and Pa8; table 3) display a transitional range of values of 44 and 279 ohm.m respectively. Comparing the trends of the gypsum pills and the one obtained for these anhydrite pills (figure 5) it is evident that the purities below 60% are dominated by the lutitic matrix and the sulphate component affects negligibly to the measure. The purities above 70% show high resistivity values in which the dominant component is the sulphate phase. For the case of gypsum pills with purity larger than 70% performed by Guinea et al. (2010b), the experiment has been repeated (samples Pg1 to Pg4; table 3) in order to measure them with the nanoammeter. The result of this repetition show an electrical resistivity values of gypsum pills lower than those obtained by Guinea et al. (2010b). Between the two differentiated trends there is a transitional zone which represents the loose of the connectivity of the matrix. As in the measures of gypsum pills by Guinea et al. (2010b), the pills with large quantity of clay component polarize with measuring time. The chargeability of clay has been widely described before (Takakura, 2006; Deucester and Kaufmann, 2009).

The percolation theory states that in a cluster with a component randomly distributed (meaning the lutitic matrix for this case) there is a percolation threshold which represent the minimal quantity of the component to display a long-range connectivity (Stauffer and Aharony, 1985). This theory has been widely used to predict characteristics of rocks as the connection of their porosity or fractures (Glover et al., 2000; Karmakar et al., 2003; Wang et al., 2007). When

the component quantity is below the percolation threshold, the cluster is no more percolant. In our system the percolation is bounded to the spreading of electrical current along the matrix which is much more conductive than the sulphate phase. Anhydrite or gypsum components are dielectric (act as resistances) and they are avoided by the electrical current while the system is percolant. When percolation threshold is surpassed, the electrical current finds no paths to spread in the matrix and it runs by the sulphates which became into conductive phases. Because of this the proportion between gypsum and anhydrite phases when the presence of matrix is above 40%, do not affect the electrical resistivity value of the whole rock.

In addition to the presence of matrix, the difference in the chemical composition between gypsum and anhydrite minerals is the presence of structural water within the crystal structure of the first one. This water forms molecular sheets which generates the main exfoliation planes (010) of gypsum crystals. This structure is not present in anhydrite crystals. The measures carried out upon gypsum crystals in different crystallographic directions display a clear difference between them (table 4). Crystal samples measured perpendicularly to the principal exfoliation planes (samples A1 to A6; table 4) show a mean resistivity of 1.5x1011 ohm.m with a standard deviation of 64%. This crystallographic direction represents the one of the anhydrite crystals. The other set of samples cut parallel to the plane (010) (samples B1 to B6; table 4) show a mean electrical resistivity of 8.9x108 ohm.m with a standard deviation of 31%. The resistivity ratio A/B is 169.7 meaning that the difference of resistivity is at least 2 orders of magnitude larger. Besides, both set of samples polarize in longtime measures; the polarization in gypsum rocks was previously described by Guinea et al. (2010a). The B samples polarize more rapidly meaning that the electrical current runs more easily. In the plane (010) the water molecules form exfoliation planes in which the hydrogen atoms create a positive electric field. This is due to that the oxygen atoms of water molecules are oriented towards to the calcium atoms of the crystalline structure while one of the hydrogen atoms of each water molecules is oriented towards to a sulphate related oxygen in the opposite part of the crystalline structure forming a weak ionic bound (figure 6A).These planes with feeble electric field facilitate the pass of electrical current in that direction.

Therefore the electrical anisotropy of gypsum crystals has been observed, showing that the electrical current spread preferentially through the main exfoliation plane. Anhydrite lacks of this exfoliation planes formed by water molecules and then it is expectable that its electrical resistivity value is larger than the one of gypsum (figure 6B). Both gypsum and

anhydrite show other exfoliation structures with preferential directions different than the principal. In the case of anhydrite the main exfoliation planes are (010), but these planes are defined by different covalent bound length of the calcium atoms with its surrounding oxygen ones. These planes do not generate such electrical anisotropies as in the case of the water-related exfoliation system.

4. THEORETICAL CALCULATIONS

4.1 Methods

Physical properties of rocks are mainly functions of their microstructure. Two dominant mathematical formalisms – effective medium theory (EMT) and percolation theory – can be used to answer this problem. The EMT (Kirpatrick, 1973) approximation is quite good for rocks with quasi-uniform distributions where only a small degree of heterogeneity is observed, although they cannot describe correctly the phenomenon of clustering (Guéguen et al., 1997) when the heterogeneity is large. Moreover, the knowledge of the geometric distribution and connectivity of the minor phase is of great importance. Percolation theory describes the medium in terms of probabilities of the connectivity but does not provide bulk physical properties. Here, we propose a method to determine the physical properties of composite materials that combines the EMT and the percolation theory. On one hand, the EMT is used to calculate the bounds of the physical properties depending on the amount of the melting phase present. These limits correspond to the two extreme situations where the melting phase is totally interconnected or disconnected. On the other hand, the percolation theory is used to determine the probability of having a connected or interconnected melting phase assuming that it is distributed in a single cube distribution.

The effective properties of composites, in particular electrical conductivity, have been studied analytically for a long time for a very simple cases (i.e Maxwell calculated the effect that a single spherical inclusion, with a different conductivity from the matrix). The rocks can be considered as random materials of different property phases at various length scales. To compute the effective properties of such materials requires knowledge of the microstructure and require numerical computation. Garboczi (1999) wrote an algorithm and the consequent FORTAN code to computed using finite difference and finite elements electrical an elastic effectives properties from a digital images of a material composed of different phases.

In this paper we have used the program ELECFEM2D.F from Garboczi to compute the effective conductivity of gypsum-anhydrite rock samples. The method to calculate the electrical conductivity value of these rocks is to analyze thin section images in which the amount of both anhydrite and gypsum proportion together with the one of the lutitic matrix is known. With this software it is possible to elaborate a resistivity distribution model based on a photograph.

In order to perform the theoretical calculation of photographs with the program ELECFEM2D.F, the pictures must be converted from HTML format (either JPG, JPEG, GIF, PNG or other image format file) into ASCII. This has been carried out with a converter which creates numerical files from the pixels of the input image. Depending on the color range of these pixels, a numeric value which is related to a user defined electrical resistivity value is assigned. As the images used display lutite, gypsum and anhydrite phases; 10, 103 and 104 ohm.m electrical resistivity values have been selected respectively. This selection will be further discussed in section 4.2. The number of variables is user defined and 2 variables (1 and 2) have been selected for photographs displaying 2 phases (any couple of lutite-gypsum-anhydrite) and 3 variables (1, 2 and 3) when the 3 of them are present. To improve the detection of each phase of the HTML/ASCII converter, each image has been treated with an image processing program in order to homogenize the color ranges.

Once the ASCII file is created, it can be run into the ELECFEM2D.F program. The ASCII files used have 150 columns and 56 rows and before being read by the program they have to be converted in a single column file. The program divides the surface into 8400 (150x56) cells with an electrical resistivity value assigned to each one and calculates the current intensity remaining after crossing the system in x or y direction. Both directions and the mean value have been calculated; the differences are related to the anisotropic distribution of the phases. The selected current has been 1 V/m, but other current intensities have been tried without altering the result.

4.2 Hashin-Shtrikman bounds for two and three phase systems

Hashin and Shtrikman (1963) defined the electrical resistivity value bounds (HS bounds) of a bulk rock only from the information of the fractions of each component. These bonds represent the maximum (upper bound) and minimum (lower bound) electrical resistivity value that a rock formed of two different phases with a certain proportion of them can display. With the knowledge of the fraction (γ) and the electrical resistivity value (ρ) of each component it is possible to calculate these upper (HS+, eq. 3) and lower bounds (HS-, eq. 4):

Equation3: $$\rho_{HS^+}{}_{1,2} = \rho_1 \left[1 - \frac{3(1-\gamma_1)(\rho_1-\rho_2)}{3\rho_1-\gamma_1(\rho_1-\rho_2)}\right]$$

Equation 4: $$\rho_{HS^-}{}_{1,2} = \rho_2 \left[1 + \frac{3\gamma_1(\rho_1-\rho_2)}{3\rho_2+(1-\gamma_1)(\rho_1-\rho_2)}\right]$$

HS bounds have been calculated for the case of gypsum rocks with different proportions of gypsum and matrix. The electrical resistivity values selected for gypsum and lutite phases have been 1000 and 10 respectively (Guinea et al., 2010b). These bounds have been compared with the general resistivity trend of the gypsum rocks (elaborated by means of field data, theoretical calculations and laboratory tests) by Guinea et al. (2010b) and the results show that they match with the lower bound when the gypsum quantity is 60% or less and with the upper bound when the gypsum purity of 70% and above (figure 7A). The values obtained between 60 and 70% in gypsum purity would be transitional, which represents the percolation threshold. Theoretically the percolation threshold is punctual but in the case of real rocks transitional values are displayed in this range of composition. In the case of anhydrite rocks (without gypsum) the same trend is expectable (figure 7B) as while the matrix percolate the sulphate phase acts as a resistance as in the case of gypsum. The electrical resistivity value selected for pure anhydrite phase has been 104 ohm.m, in accordance with the maximum value measured in field examples and the bibliography. The trend has been supported by the results of the laboratory measures in pills and the field measures with ERT.

A general form of the bounds for n-phases was given by Berriman (1995). With his formulae it is possible to elaborate ternary graphics for 3-phased rocks (Ledo and Jones, 2005). Gypsum-Anhydrite-Lutite (GAL) system has been calculated for both lower (eq. 5) and upper (eq. 6) HS bounds:

Equation 5: $$\rho_{HS^+}{}_{gy,anh,lu} = \frac{1}{\left(\frac{\gamma_{gy}}{\rho_{gy}+2\rho_{lu}}\right)+\left(\frac{\gamma_{lu}}{3\rho_{lu}}\right)+\left(\frac{\gamma_{anh}}{\rho_{anh}+2\rho_{lu}}\right)} - 2\rho_{lu}$$

Equation 6: $$\rho_{HS^-}{}_{gy,anh,lu} = \frac{1}{\left(\frac{\gamma_{gy}}{\rho_{gy}+2\rho_{anh}}\right)+\left(\frac{\gamma_{lu}}{\rho_{lu}+2\rho_{anh}}\right)+\left(\frac{\gamma_{anh}}{3\rho_{anh}}\right)} - 2\rho_{anh}$$

In the case of lower bound (figure 8A), the system is clearly dominated by the lutitic component; the isoresistivity lines are parallel between them showing no appreciable variation in the gypsum-anhydrite axis but when the lutite component is less than 10%. The values of

resistivity are very low in general, showing less than 100 ohm.m for a sulphate purity of 70%. The upper bound (figure 8B) displays a very different trend dominated by the anhydrite component, but in this case the 3 components affect the bulk resistivity value of the rock. The electrical resistivity values are much larger than in the case of lower bound achieving 1000 ohm.m with only 40% of anhydrite. As it has been previously shown, the electrical behavior of the rocks is the one of lower HS bound when the quantity of matrix is above 40% and the one of upper bound when is below 30%. Thus it is expectable that the real distribution of the electrical resistivity for the GAL system should be a combination between the upper and lower HS bounds (figure 8C).

4.3 Results and discussion

In order to check the accurateness of this GAL diagram, the theoretical electrical resistivity value of real thin section rock photographs (figure 9) has been calculated with ELECFEM2D program. Lutitic matrix display brownish coloring while both anhydrite and gypsum have are transparent underplane polarized light; having anhydrite higher relief than gypsum (its bounds are well marked with dark lines). With crossed polarized light, gypsum and anhydrite can be easily differentiated because of the different coloring of the anhydrite (pink, green, blue, …) in contrast with the gray colors of the gypsum crystals. The standard electrical resistivity values selected for the gypsum, anhydrite and lutitic matrix phases have been 103, 104 and 10 ohm.m respectively, as has been assigned before. The electrical resistivity of the bulk sections has been measured in both x and y directions; when the distribution of the components is homogeneous these values would be considered similar. For each thin section the fractions of the components are calculated by the program so it is possible to obtain the electrical resistivity value corresponding to these fractions calculated with Hashin-Shtrikman bounds (table 5).

The results show that the mean of the calculated electrical resistivity values in x and y directions are in general close to HS+ bound when the quantity matrix is lower than 30% (figure 9, thin sections A, D, E, F, G and H; table 5) and to the HS- bound when the quantity of matrix is abundant (figure 9, B and I; table 5). There is a good match between the corresponding position of each sample in the figure 8C, according to their components percentages, and the calculated resistivity values. In the case of thin sections C and J there is abundant matrix (58 and 52% respectively); nevertheless, the calculated resistivity values are slightly larger than that expected for such mixture. This is due to that the phases are not

scattered and randomly distributed within the samples but forming compact and pure areas. This represents large heterogeneities which change the percolating behavior (we have considered it only for regular distributions of the phases as in the case of the pills) of the bulk rock and makes the transition zone larger. In any case the values are always much closer to the lower bound that to the upper one.

At larger scale (as in the ERT profiles) the rocks are in general more homogeneous and should fit to the HS lower bound for compositions of 0-60% in lutitic matrix. The microscopic anisotropies do not affect to the electrical conductivity of the bulk deposit if we increase the scale. In any case, it is possible to observe cases of heterogeneities at metric scale. When these heterogeneities are large, they can be considered as different rocks (for example a gypsum-rich lutite body within a larger pure gypsum host-rock). In any case, heterogeneities below the detection limit of the method will be considered as a single rock. Another possible case is a layered deposit in which every layer has different purity in the sulphate phase. If the difference among purities is low, which is the most common case, the whole sequence can be considered as a single member with a mean purity. Rarely sulphate deposits have great variations of purity from layer to layer forming a heterogeneous sequence. Sudden variations in the purity exist, but normally are associated to the limit of a sequence or a stable change in the deposition conditions. In the case of having layering between almost pure matrix and highly pure sulphates, the transitional values of resistivity will increase their range as happens in the case of the microphotographs.

5 GEOELECTRICAL CLASSIFICATION OF CALCIUM SULPHATE ROCKS

With the GAL diagram obtained combining both HS+ and HS- boundaries for a gypsum anhydrite-lutite system (figure 8C) a geoelectrical classification has been elaborated differentiating 6 calcium sulphate rock types (figure 10). When the lutitic matrix is connected at long range (in the case of sulphate purity lower than 60%) the system is matrix dominant and therefore there is no possibility of differentiating between gypsum and anhydrite component; these rocks are classified as Lutites and Gypsum/Anhydrite rich Lutites. The electrical resistivity of this groups range from 10 to 100 ohm.m. When the sulphate purity is larger than 70%, the rock will be considered as Pure Gypsum when it ranges from 700 to 1000 ohm.m as was stated by Guinea et al. (2010b) for the case of gypsum-lutite systems. If the sulphate mineral is mainly anhydrite (more than 90%) the rock is considered Pure Anhydrite

and its electrical resistivity value range from 2500 to 104 ohm.m depending on the rock purity. In the case of presence of both gypsum and anhydrite sulphate phases, the rock is considered Gypsum with Anhydrite (1000 to 2000 ohm.m) or Anhydrite with Gypsum (2000 to 5000 ohm.m). The values of pure Anhydrite and Anhydrite with Gypsum overlap; in this case it is possible to bond the electrical value to Pure Anhydrite rocks when there are no evidences of rehydration and to the Anhydrite with Gypsum in the contrary case. Between Lutites and Gypsum/Anhydrite rich Lutites and the sulphate pure rocks there is a transitional area displaying transitional values from 100 to 700/2500 ohm.m (depending of the sulphate composition). The lower boundary of Transitional Gypsum/Anhydrite rocks has been selected for 55% in sulphate purity instead 60% because the measures in pills have shown that the 60% values display an electrical resistivity increasing trend; the upper boundary is 70% in gypsum purity.

For the case of microscopic scale, it has been shown that the transitional range is wider (including rocks between 30 and 55% in sulphate purity, depending of the anisotropy). For the cases of purities higher than 70% or smaller than 30%, the obtained values are similar to the corresponding HS bound. At larger scale, the ERT lines have shown relations between composition and resistivity values similar to the ones displayed in the classification of the figure 10; this is, higher than 5000 ohm.m when the dominant phase is the anhydrite, 1500 to 5000 ohm.m for different proportions of gypsum and anhydrite (with presence of little lutite) and close to 1000 ohm.m when the gypsum is the dominant phase. For deposits with large amount of lutites, the obtained value has been <60 ohm.m in all cases.

6. CONCLUSIONS

The electrical behavior of calcium sulphate rocks has been widely studied at different scales with crystals, microphotographs, synthetic pills and geological deposits. Laboratory tests in pills have shown that the matrix of calcium sulphate rocks is affected by the percolation phenomena and therefore, when the matrix quantity in a rock is greater than 40% the electrical current avoids the sulphate minerals. The percolation threshold is defined for the stretch of 60-70% in sulphate purity; when this purity is larger, the sulphate minerals are the ones conditioning the electrical resistivity of the bulk rock. The electrical resistivity of gypsum crystals is lower in the direction of the main exfoliation planes due to the electric field

generated by the water molecules; this explains the reason of the larger resistivity of anhydrite, which lacks of this water exfoliation layers.

The electrical resistivity value of anhydrite rocks range from 10 to 104 ohm.m; being the larger values related to purest rocks. This value is found in the field examples where the anhydrite appears as massive. The values observed in rocks with both gypsum and anhydrite (with minor matrix) have ranged between 1500 and 5000 ohm.m depending on the quantity of each other. Large quantity of matrix in sulphate rocks have shown low electrical resistivity values been unable to differentiate between gypsum and anhydrite.

When the matrix of the calcium sulphate rocks is percolant (more than 40%), the electrical resistivity value fits with the value calculated with the Hashin-Shtrikman lower bound (HS-), and when is embedded in the sulphate phase (30% of matrix or less) fits with the Hashin-shtrikman upper bound (HS+). If there are large heterogeneities in the distribution of the phases, the resistivity values of rocks with a matrix quantity close to 50% can display transitional values (more than 100 ohm.m, without reaching values of the purest sulphate rocks). Therefore, it is possible to calculate any combination of these 3 components and the geoelectrical classification has been elaborated for calcium sulphate rocks. With this classification is possible to determine the purity of the sulphates and the presence of anhydrite in gypsum rocks, which is useful for the characterization of the deposit.

The study of these rocks is interesting also as reference for the studies of other rocks formed of various components with differentiated electrical resistivity values, as for example a lime-sand-gravel system. With similar methods to the ones used in this survey, it should be possible to predict the electrical resistivity of these rocks depending on their composition.

ACKNOLEDGEMENTS

The present work is a part of a PhD thesis supported by the “Programa General d’Intensificació de la Recerca” (Generalitat de Catalunya-UB) and the Spanish Government Projects CGL2009-11096, CGL2009-07025, CGL2010-18260 and CGL2009-07604. We want to appreciate the support and facilities of Drs. Albert Casas, Esperança Tauler and Manel Labrador (Universitat de Barcelona, UB) and Dr. Ricard Bosch (Universitat Politècnica de

Barcelona, UPC). We also want to thank to Grupo Uralita Corporation, especially to Ms. Mayte Martín, for letting us work in the quarry of Beuda and their support.

REFERENCES:

Asfahani, J., Mohamad, R., 2002. Geo-electrical investigation for sulphur prospecting in Teshreen Structure in Northeast Syria. Exploration and Mining Geology, 11, 49-59.

Ayora, C., García-Veigas, J., Pueyo, J.J., 1994. The chemical and hydrological evolution of an ancient potash-forming evaporite basin as constrained by mineral sequence, fluid inclusion composition and numerical simulation. Geochimica et Cosmochimica Acta, 58, 3379-3394.

Berriman, J.G., 1995. Mixture theories for rock properties. In: T.J. Ares Ed., Rock Physics and Phase Relations: A Handbook of Physical Constants. American Geophysical Union, Washington, 236pp.

Bleaney, B.I., Bleaney, B., 1976. Electricity and Magnetism 3rd Edition. Great Britain: Oxford University Press, 63pp.

Carrillo, E., 2009. Unidades evaporíticas eocenas de la Zona Surpirenaica Oriental (Área de La Garrotxa). Geogaceta, 47, 73-76.

Chouteau, M., Phillips, G., Prugger, A., 1997. Mapping and monitoring softrock mining. In: Proceedings of Exploration 97: Fourth Decennial International Conference of Mineral Exploration, A.G. Gubins Ed., 927-940.

Daily, W., Ramirez, A., LaBrecque, D., Barber, W., 1995. Electrical resistance tomography experiments at the Oregon Graduate Institute. Journal of Applied Geophysics, 33, 227-237.

deGroot-Hedlin, C., Constable, S., 1990. Occam's inversion to generate smooth, two-dimensional models from magnetotelluric data. Geophysics, 55, 1613-1624.

Deucester, J.& Kaufmann, O., 2009. Correlation between inverted chargeabilities and organic compounds concentrations in soils-A field experiment. 15th Near Surface meeting, Dublin, Ireland, Expanded Abstracts, C19.

Ewanic, M., Reichhardt, D., Brunet, B.S., 2001. Electrical Resistivity Tomography Imaging of a Colloidal Silica Grout Injection. Containment Remediation Technology, Abstract 137.

Furman, A., Ferré, P.A., Warrik, A.W., 2003. A Sensitivity Analysis of Electrical Resistivity Tomography Array Types Using Analytical Element Modeling. Vadose Zone Journal, 2, 416-423.

Garboczi, E.J., 1999. Finite element and finite difference programs for computing the linear electric and elastic properties of digital images of random materials. NIST Internal Report 6269. Also available at http://ciks.cbt.nist.gov/garbocz/

Giao, P.H., Chung, S.G., Kym, D.Y., Tanaka, H., 2003. Electric imaging and laboratory resistivity testing for geotechnical investigation of Pusan clay deposits. Journal of Applied Geophysics, 52, 157-175.

Glover, P.W.J., Hole, M.J., Pous, J., 2000. A modified Archie's law for two conducting phases. Earth and Planetary Science Letters, 180, 369-383.

Guéguen, Y., Chelidze, T., Le Ravalec, M., 1997. Microstructures, percolation thresholds, and rock physical properties. Tectonophysics, 279, 23-35.

Guinea, A., Playà, E., Rivero, L., Salvany, J.M., Himi, M., 2009. Geoelectrical imaging supporting glauberite deposits evaluation in the Montes de Torrero area (Zaragoza). Geogaceta, 47, 145-148.

Guinea, A., Playà, E., Rivero, L., Himi, M., 2010a. Electrical Resistivity Tomography and Induced Polarization techniques applied to the identification of gypsum rocks. Near Surface Geophysics, 8, 249-257.

Guinea, A., Playà, E., Rivero, L., Himi, M., Bosch, R., 2010b. Geoelectrical Classification of Gypsum Rocks. Surveys in Geophysics, 31 (6), 557-580.

Halpern, A., 1998. Schaum's Outlines Beginning Physics II. New York: McGraw-Hill Companies Inc., 141pp.

Hashin, Z., Shtrikman, S., 1963. A variational approach to the theory of the elastic behavior of multiphase materials. Journal of the Mechanics and Physics of Solids, 11, 12-140.

Inglés, M., Manote, M.R., Ortí, F., Pey, J., Playà, E., Rosell, L., Yeguas, J., 2009. Geochemical methods in alabaster provenance: an application example. IX ASMOSIA: Interdisciplinary Studies on Ancient Stone meeting, Tarragona, Spain, Abstracts 125.

Jakosky, J.J., 1950. Exploration geophysics. Trija Publishing Co., Los Angeles, 1195pp.

Karmakar, R., Manna, S.S., Dutta, T., 2003. A geometrical model of diagenesis using percolation theory. Physica A, 318, 113-120.

Keller, G.V., 1966. Electrical properties of rocks and minerals. In: Clark S.P. (Ed.), Handbook of physical constants. The Geological Society of America, 587pp.

Kirkpatrick, S., 1973. Percolation and conduction. Reviews of Modern Physics, 45, 574-588.

Klein, C., Hurlburt, C.S., 1998. Manual de mineralogía de Dana. Reverté, 438pp.

Ledo, J., Jones, A.G., 2005. Upper mantle temperature determined from combining mineral composition, electrical conductivity laboratory studies and magnetotelluric field observations: Application to the intermontane belt, Northern Canadian Cordillera. Earth and Planetary Science Letters, 236, 258-268.

Loke, M.H., Baker, R.H., 1996. Rapid least-squares inversion of apparent resistivity pseudosections by a quasi-Newton method. Geophysical Prospecting, 44, 131-152.

Lugo, E., Playà, E., Rivero, L., 2008. Aplicación de la tomografía eléctrica a la prospección de formaciones evaporíticas. Geogaceta, 44, 223-226.

Ma, Y., Wang, H., Xu, L.A., Jiang, C., 1997. Simulation study of the electrode array used in an ERT system. Chemical Engineering Science, 52, 2197-2203.

Norma española UNE 21-303-83, 1983. Métodos para la medida de la resistividad transversal y superficial de los materiales aislantes eléctricos sólidos. Instituto Español de Normalización.

Ortí, F., 2000. Unidades glauberíticas del Terciario ibérico: nuevas aportaciones. Revista de la sociedad geológica de España, 13, 227-249.

Ortí, F., Rosell, L., Playà, E., García-Veigas, J., 2010. Large gypsum nodules in the Tertiary evaporites of Spain: distribution and paleogeographic significance. Geological Quarterly, 54 (4), 411-422.

Parkhomenko, E.J., 1967. Electrical properties of rocks. Plenum Press, New York, 314pp.

Rider, M.H., 1986. The Geological interpretation of well logs. Blackie Halsted Press, 175pp.

Robinson, E.S., Çoruh, C., 1988. Basic Exploration Geophysics. Jonh Wiley and sons, 562pp.

Rosell, L., Pueyo, J.J., 1997. Second marine evaporitic phase in the South Pyrenean Foredeep: the priabonian potash basin (Later Eocene: Autochthonous-Allochthonous Zone). In: Busson, G., Schreiber, Ch. Eds. Sedimentary deposition in rift and foreland basins in France and Spain. Columbia University Press, New York, 358–387.

Rusell, E.J.F., Barker, R.D., 2010. Electrical properties of clay in relation to misture loss. Near Surface Geophysics, 8, 173-180.

Salvany, J.M., 2009. Geología del yacimiento glauberítico de Montes de Torrero (Zaragoza). Prensas Universitarias de Zaragoza, 72pp.

Sasaki, Y., 1992. Resolution of resistivity tomography inferred from numerical simulation. Geophysical Prospecting, 40, 453-46.

Stauffer, D., Aharony, A., 1985. Introduction to percolation theory. Taylor and Francis (Eds.), 181pp.

Szalai, S., Szarka, L., 2008. On the classification of surface geoelectric arrays. Geophysical Prospecting, 56, 159-175.

Takakura, S., Nakada, K., 2006. IP measurements on tunnel walls of a sericite deposit – A contact method of nonpolarizable electrodes on a base rock and detection of clay minerals by normalised chargeability. Geophysical Exploration, 59, 363–370.

Telkes, M., 1950. Thermoelectric power and electrical resistivity of minerals. American Mineralogist, 35, 536-555.

Tomioka, H., Yoshizawa, H., Suzuki, K., Milman, Y.V., Krapivka, N.A., Hashimoto, I., 1998. Electrical Resistivity of High Purity Chromium Single Crystal. Physica Status Solidi (a), 167, 443-448.

Vanhala, H., Lintinen, L., Ojala, A., 2009. Electrical Resistivity Study of Permafrost on Ridnitšohkka Fell in Northwest Lapland, Finland. Geophysica, 45(1–2), 103–118.

Wang, K.W., Sun, J.M., Guan, J.T., Zhu, D.W., 2007. A percolation study of electrical properties of reservoir rocks. Physica A, 380, 19–26.

Zou, M., Pecharsky, V.K., Gschneidner Jr., K.A., Mudryk, Y., Schlagel, D.L., Lograsso, T.A., 2009. Electrical resistivity and magnetoresistance of single-crystal Tb5Si2.2Ge1.8. Physical Review B, 80, 174411.

TABLE CAPTIONS

Table 1: Geoelectrical classification of gypsum rocks (modified from Guinea et al. 2010b).

Table 2: Published electrical resistivity values for anhydrite rocks.

Table 3: Results of the laboratory measures in the synthetic pills made of a mixing of powdered pure anhydrite or gypsum reagents and clay. The samples with larger purities in sulphates (Pa7,Pa8, Pa9, Pa10, Pg1, Pg2, Pg3 and Pg4) have been measured with a nanoammeter instead of a microammeter.

Table 4: Result of the laboratory measures in crystal sheets. A samples are cut parallel to the main exfoliation planes (010) and B samples are perpendicularly to them.

Table 5: Results of the theoretical calculations of electrical resistivity of the thin section photographs with ELECFEM2D software. The result of the measures in both x and y directions as well as the mean resistivity values are listed. Lower (HS-) and upper (HS+) Hashin-Shtrikman bounds have been also calculated, only considering the proportion of each phase. The corresponding image of the thin sections A to J are displayed in the figure 9.

FIGURE CAPTIONS

Figure 1: Distribution of evaporite formations in the Tertiary basins northeastern Spain indicating the location of the nine studied ERT profiles with red dots (modified from Ortí et al., 2010).

Figure 2: Photographs of the areas studied with ERT, A to F are taken in the quarry of Beuda while G is taken in the area of Odena and H in Zaragoza formation. A) general view of the quarry; B) pure gypsum-anhydrite boundary with a interdigitation between them; C) sulphate layers showing less purity than in other areas; D) boundary between pure anhydrite and relatively impure gypsum; E) anhydrite blocks filled with gypsum veins and embedded in a gypsum matrix; F) massive anhydrite with little gypsum within; G) massive anhydrite body; H) impure sulphate layers in Montes de Torrero area.

Figure 3: Inverted data of the electrical resistivity tomography lines for the different areas studied (the location of the profiles is showed in figure 6). Profile I modified from Guinea et al. (2010b).

Figure 4: Electrical device to measure the electrical resistivity values of the samples; it consists of a switchable laboratory power-supply, two electrodes and an ammeter (micro or nanoammeter depending on the samples). A) general scheme and sketch of the circuit; B) Electrode disposition for measures in crystal sheet samples, where the electric contact is made with conductive gel in a surface delimited with insulating tape.

Figure 5: Semi-logarithmic plot representing the results of the measures in anhydrite-clay pills and compared to the results obtained for gypsum-clay pills by Guinea et al (2010b). The resistivity values for the highest gypsum pills has been recalculated after measuring with a nanoammeter.

Figure 6: A) Detail of the atom and charge distribution in the water layers of gypsum crystals displayed in figure 7 (the crystallographic axis are turned 90º); B) crystallographic structure of anhydrite.

Figure 7: Hashin-Shtrikman bounds for two phase case. A) HS bounds for gypsum rocks and the trend showed by Guinea et al. (2010b); B) HS bounds for anhydrite rocks and the expected trend of electrical resistivity value.

Figure 8: Ternary plots showing Hashin-Shtrikman bounds for gypsum-anhydrite-lutite (GAL) system. A) lower HS bound; B) upper HS bound; C) combined diagram considering the percolation phenomena.

Figure 9: Microphotographs of thin section of calcium sulphate rocks. D, E, H and I are taken with cross polarized light and the rest with plane polarized light. The different phases are indicated with numbers 1 (gypsum), 2 (anhydrite) and 3 (lutite/carbonate).

Figure 10: Geoelectrical classification of calcium sulphate rocks, depending on their gypsum-anhydrite-lutite contents. In the background is displayed in gray lines the resistivity value trend showed in figure 10C.

TABLE.1

	Purity in Gypsum (%)	Resistivity (ohm.m)
Lutites and Gypsum rich Lutites	0-55	10-100
Transitional Gypsum	55-75	100-700
Pure Gypsum	75-100	700-1000

TABLE.2

REFERENCE	RESISTIVITY (ohm.m)	AUTHOR'S COMMENTS
Lugo et al. (2008)	1000-11500	The bodies displaying the lowest values are related to the presence of gypsum from the hydration of anhydrite while the highest ones are related to pure anhydrite.
Asfahani and Mohammad (2002)	94-1200	The values are measured by vertical electrical soundings in a gypsum and anhydrite formation.
Choteau et al. (1997)	1000	Anhydrite appears in an halite-karnalite-tachyhydrite secuence.
Robinson and Çoruh (1988)	10^9-10^{10}	Anhydrite appears in a summary of different mineral resistivity values
Rider (1986)	10^4-10^{10}	Obtained from diagraphy logs of different sources.
Parkhomenko (1967)	1.0 -10^9	Listed in a summary of different mineral and rock resistivities
Jakosky (1950)	1.0 -10^3 / 1.0-10^5	Low and High resistivity ranges obtained from laboratory measures

TABLE.3

Sample	% Sulphate	Thickness (cm)	Voltage (V)	Measure (µA)	Resistivity (ohm.m)
Pa1	0	0.455	1.5	96	6
Pa2	10	0.470	1.5	78	7
Pa3	20	0.475	1.5	62	9
Pa4	30	0.490	1.5	48	11
Pa5	40	0.490	1.5	34	16
Pa6	50	0.490	1.5	26	21
Pa7	60	0.500	1.5	12	44
Pa8	70	0.520	0.1	0.122	279
Pa9	80	0.540	1	0.175	1870
Pa10	90	0.530	1	0.074	4505
Pa11	100	0.505	1	0.026	13457
Pg1	70	0.500	0.1	0.160	221
Pg2	80	0.510	0.1	0.130	267
Pg3	90	0.510	0.1	0.090	385
Pg4	100	0.505	0.2	0.082	853

TABLE.4

Sample	Thickness (cm)	Electrode area (cm2)	Voltage (V)	Essay 1 (nA)	Essay 2 (nA)	Essay 3 (nA)	Essay 4 (nA)	Essay 5 (nA)	Mean resistivity (ohm.m)
A1	0.125	3.00	1	21	25	11	17	13	1.40E+11
A2	0.100	2.90	1	10	7	9	13	11	2.90E+11
A3	0.070	3.00	1	28	7	16	15	21	2.50E+11
A4	0.080	0.80	1	19	22	34	37	17	3.90E+10
A5	0.050	1.05	1	37	8	17	22	13	1.10E+11
A6	0.040	0.98	1	14	44	32	34	22	8.30E+10
B1	0.415	2.16	0.1	74	81	83	73	66	6.90E+08
B2	0.575	3.22	0.1	49	68	42	95	54	9.10E+08
B3	0.635	3.08	0.1	38	52	60	72	36	9.40E+08
B4	0.360	3.75	0.1	78	82	61	106	48	1.40E+09
B5	0.375	1.60	0.1	39	66	52	70	61	7.40E+08
B6	0.490	2.00	0.1	48	59	64	54	83	6.60E+08

TABLE.5

Thin section	%Gy	%Anh	%Lut	HS- (ohm.m)	HS+ (ohm.m)	X (ohm.m)	Y (ohm.m)	Mean (ohm.m)
A	95	0	5	365	928	862	844	853
B	17	0	83	16	129	16	16	16
C	0	42	58	32	1091	214	126	170
D	0	83	17	154	4504	3087	3157	3122
E	29	71	0	2796	4417	5070	6024	5547
F	68	32	0	1411	1947	1622	2265	1944
G	26	51	23	105	2105	1102	2474	1788
H	53	34	13	185	1708	1129	1940	1535
I	35	6	59	30	408	33	82	58
J	38	10	52	36	540	65	210	138

FIGURE.1

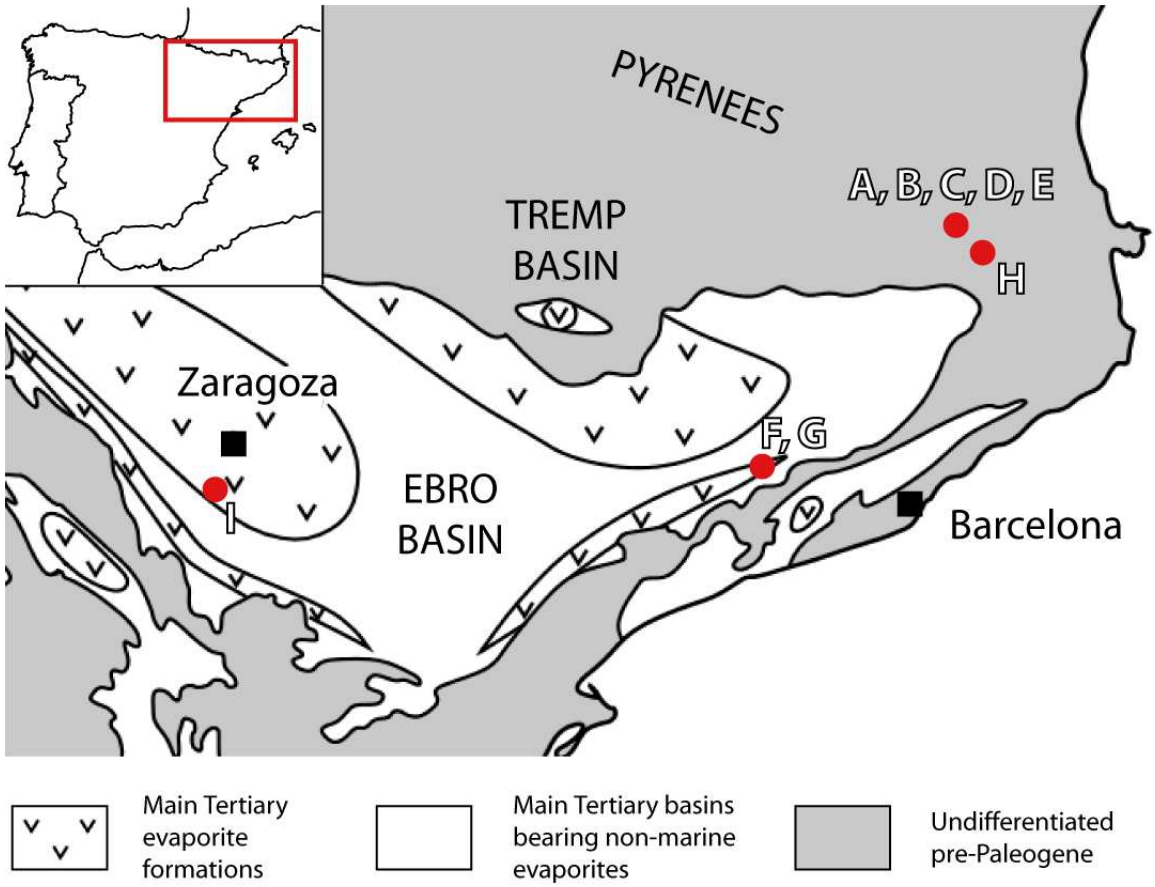
PYRENEES
A, B, C, D, E
TREMP
BASIN
H
Zaragoza
F, G
EBRO
BASIN
I
Barcelona
Main Tertiary evaporite formations
Main Tertiary basins bearing non-marine evaporites
Undifferentiated pre-Paleogene

FIGURE.2

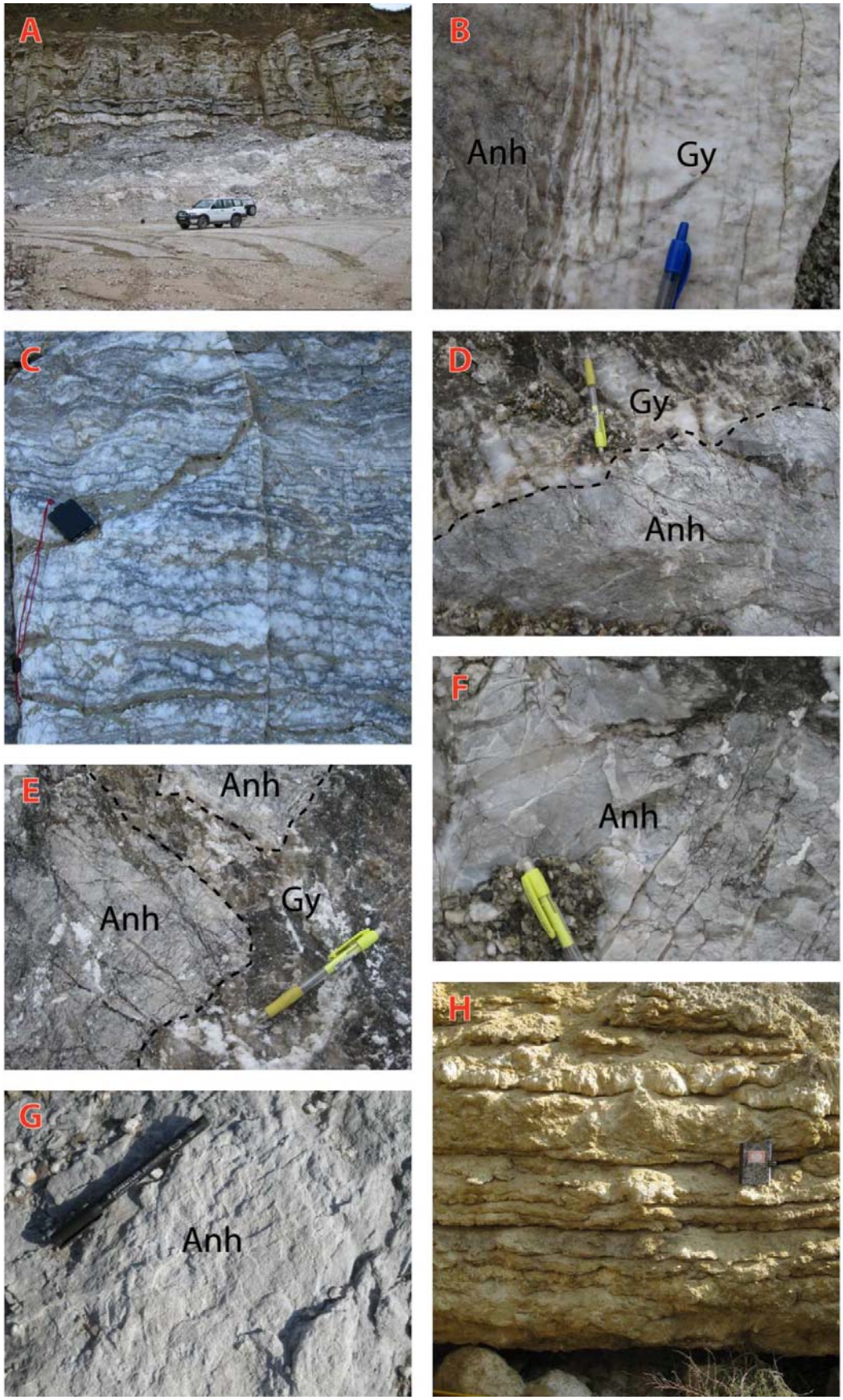

FIGURE.3

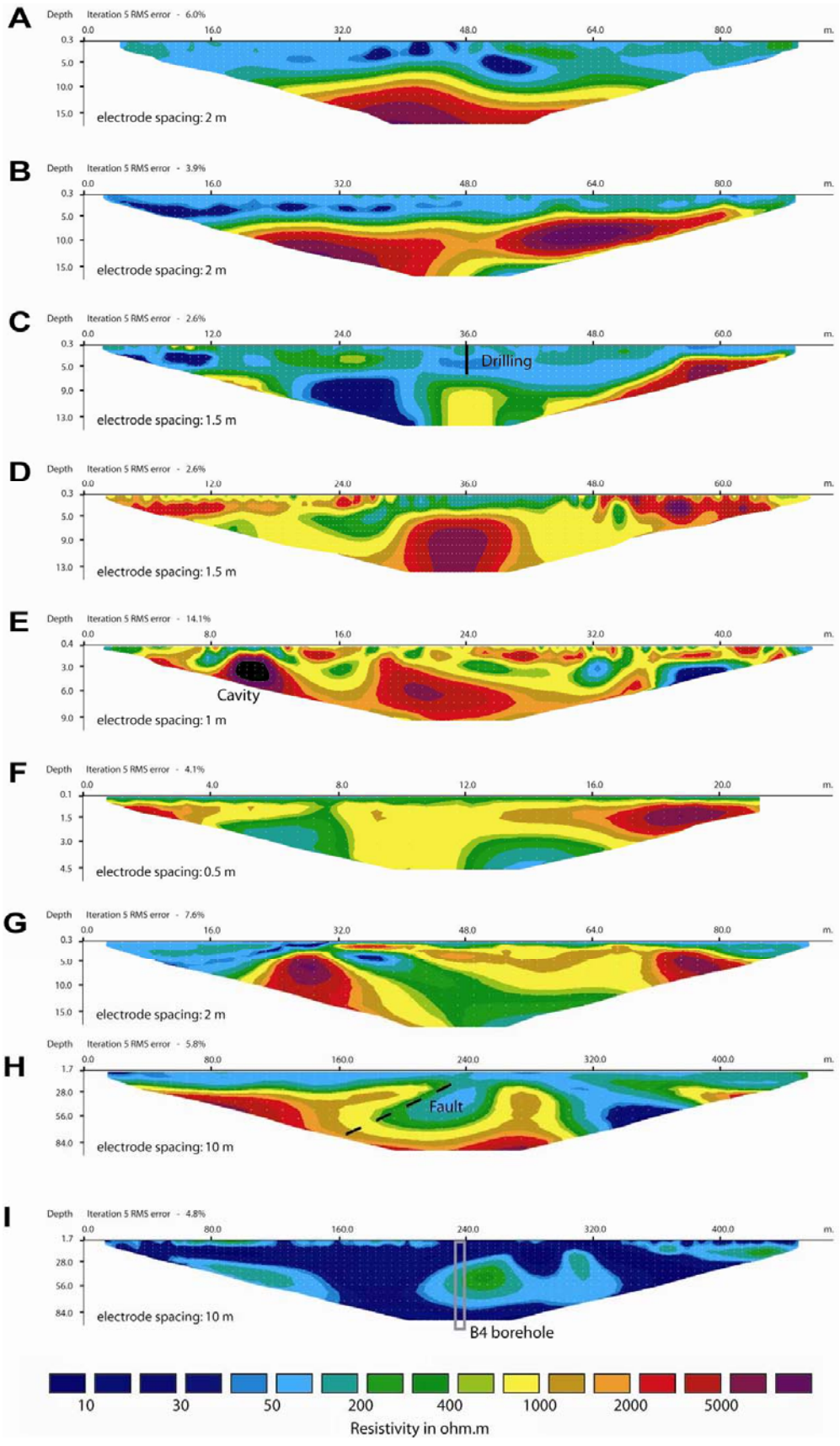
A
Depth Iteration 5 RMS error - 6.0%
0.0 16.0 32.0 48.0 64.0 80.0 m.
0.3
5.0
10.0
15.0
electrode spacing: 2 m
B
Depth Iteration 5 RMS error - 3.9%
0.0 16.0 32.0 48.0 64.0 80.0 m.
0.3
5.0
10.0
15.0
electrode spacing: 2 m
C
Depth Iteration 5 RMS error - 2.6%
0.0 12.0 24.0 36.0 48.0 60.0 m.
0.3
5.0
9.0
13.0
Drilling
electrode spacing: 1.5 m
D
Depth Iteration 5 RMS error - 2.6%
0.0 12.0 24.0 36.0 48.0 60.0 m.
0.3
5.0
9.0
13.0
electrode spacing: 1.5 m
E
Depth Iteration 5 RMS error - 14.1%
0.0 8.0 16.0 24.0 32.0 40.0 m.
0.4
3.0
6.0
9.0
Cavity
electrode spacing: 1 m
F
Depth Iteration 5 RMS error - 4.1%
0.0 4.0 8.0 12.0 16.0 20.0 m.
0.1
1.5
3.0
4.5
electrode spacing: 0.5 m
G
Depth Iteration 5 RMS error - 7.6%
0.0 16.0 32.0 48.0 64.0 80.0 m.
0.3
5.0
10.0
15.0
electrode spacing: 2 m
H
Depth Iteration 5 RMS error - 5.8%
0.0 80.0 160.0 240.0 320.0 400.0 m.
1.7
28.0
56.0
84.0
Fault
electrode spacing: 10 m
I
Depth Iteration 5 RMS error - 4.8%
0.0 80.0 160.0 240.0 320.0 400.0 m.
1.7
28.0
56.0
84.0
electrode spacing: 10 m
B4 borehole
10 30 50 200 400 1000 2000 5000
Resistivity in ohm.m

FIGURE.4

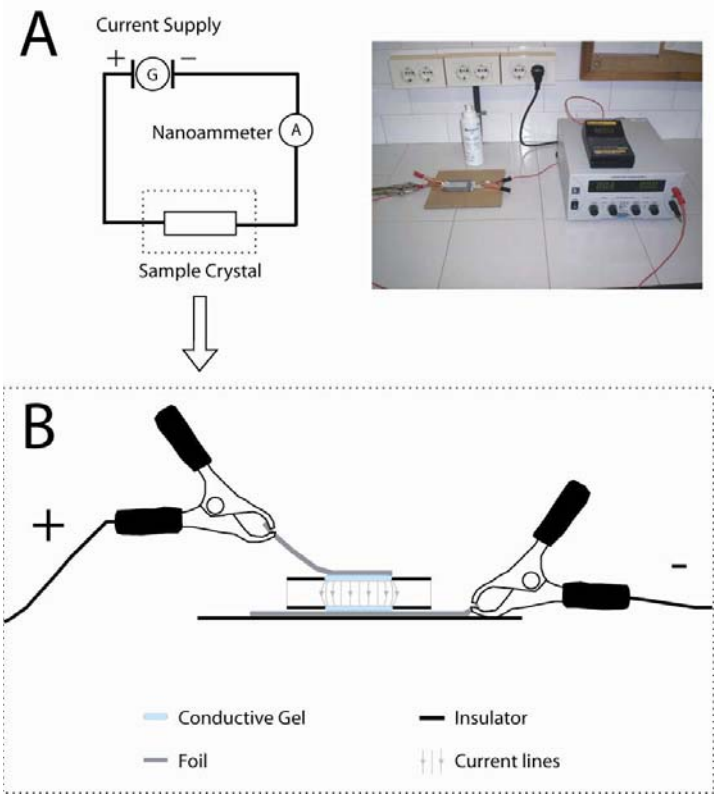

FIGURE.5

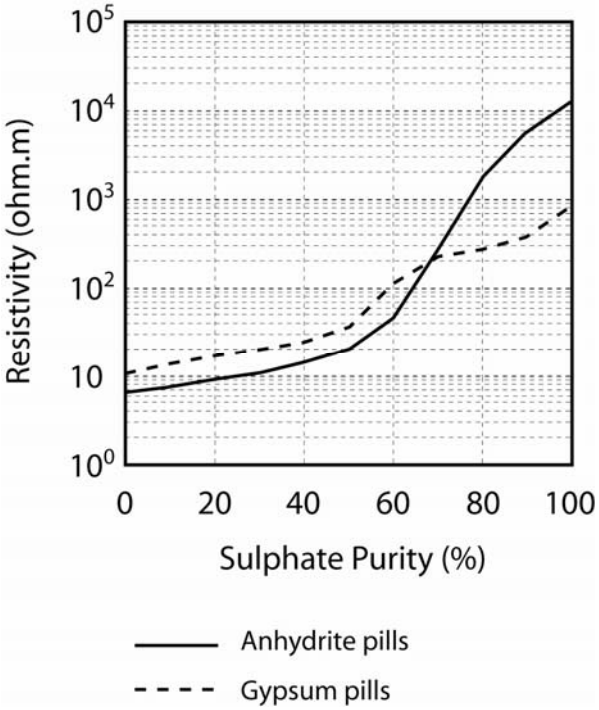

FIGURE.6

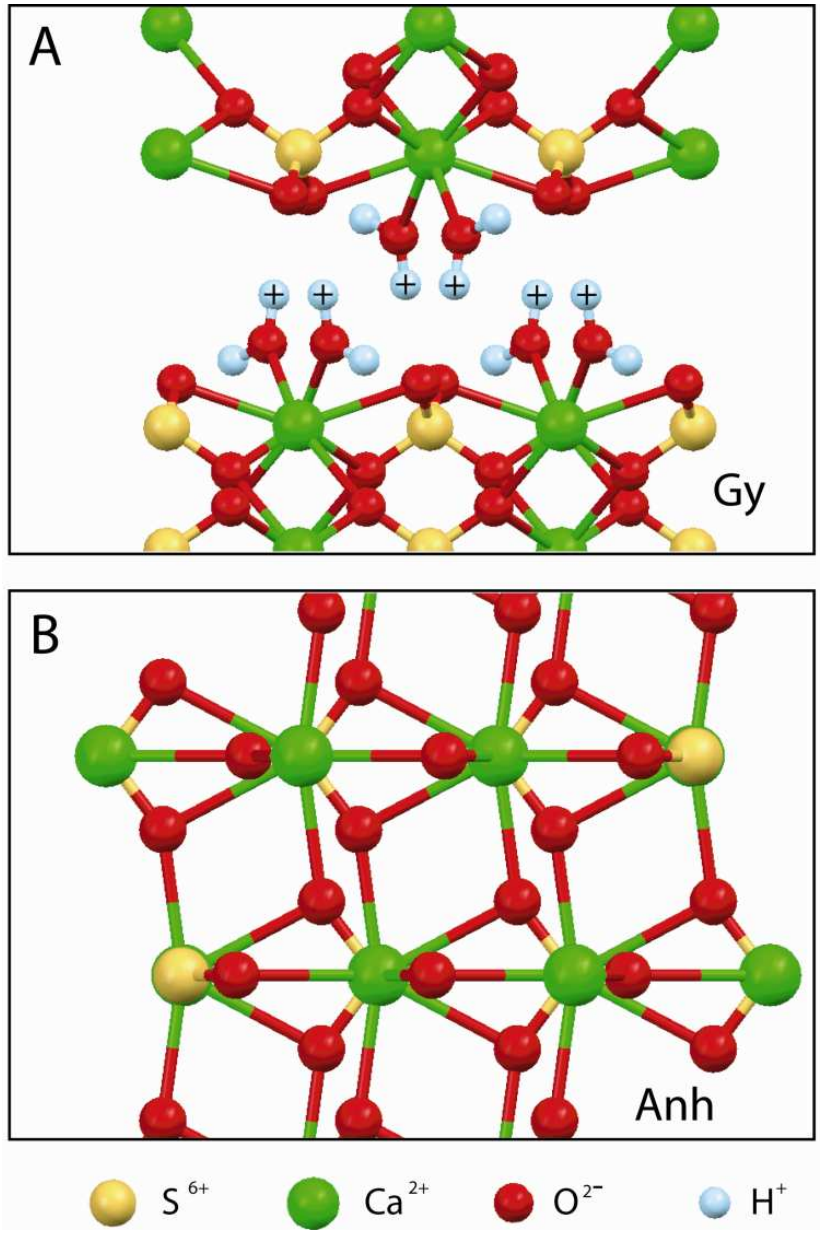

FIGURE.7

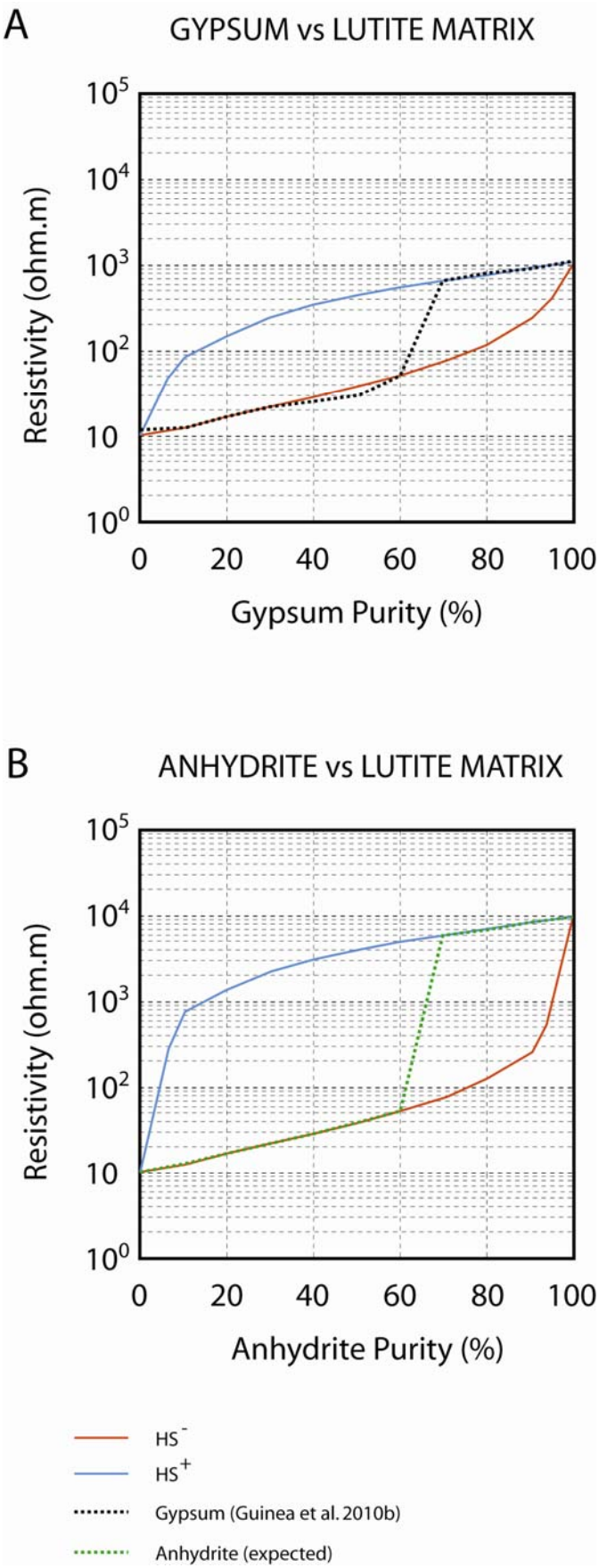
A
GYPSUM vs LUTITE MATRIX
Resistivity (ohm.m)
10^5
10^4
10^3
10^2
10
10^0
0
20
40
60
80
100
Gypsum Purity (%)
B
ANHYDRITE vs LUTITE MATRIX
Resistivity (ohm.m)
10^5
10^4
10^3
10^2
10
10^0
0
20
40
60
80
100
Anhydrite Purity (%)
HS^-
HS^+
Gypsum (Guinea et al. 2010b)
Anhydrite (expected)

FIGURE.8

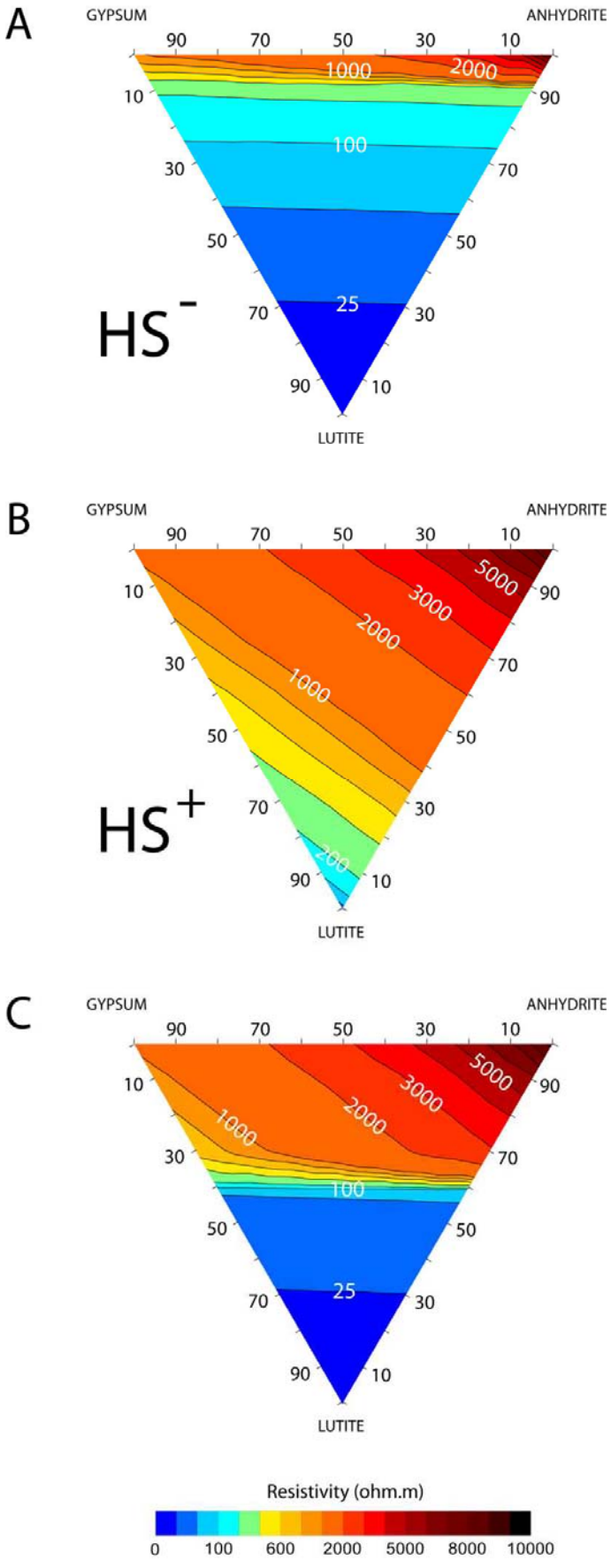
A
GYPSUM
ANHYDRITE
LUTITE
1000
2000
100
25
HS⁻
B
GYPSUM
ANHYDRITE
LUTITE
5000
3000
2000
1000
200
HS⁺
C
GYPSUM
ANHYDRITE
LUTITE
5000
3000
2000
1000
100
25
Resistivity (ohm.m)
0
100
600
2000
5000
8000
10000

FIGURE.9

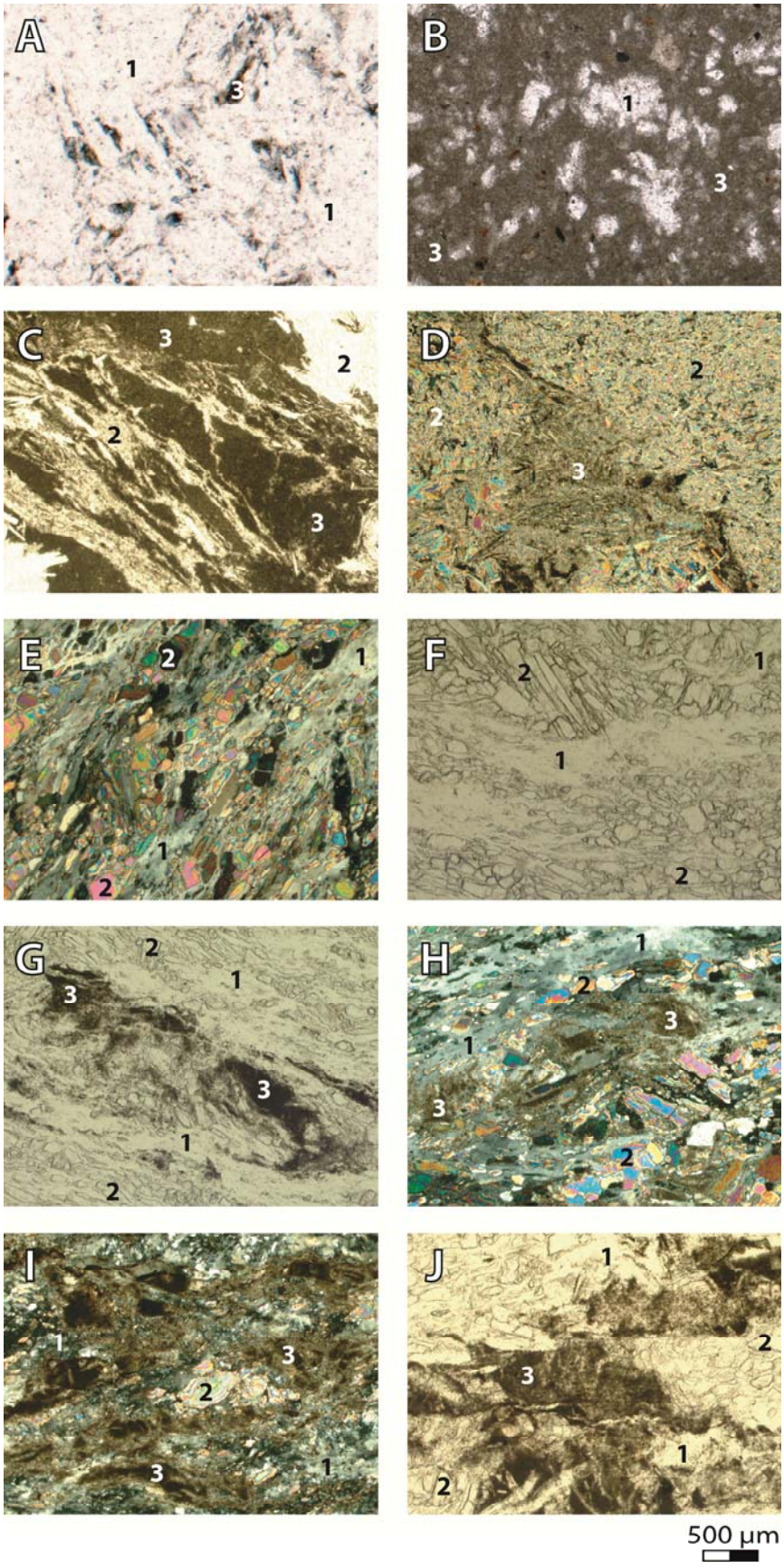

FIGURE.10

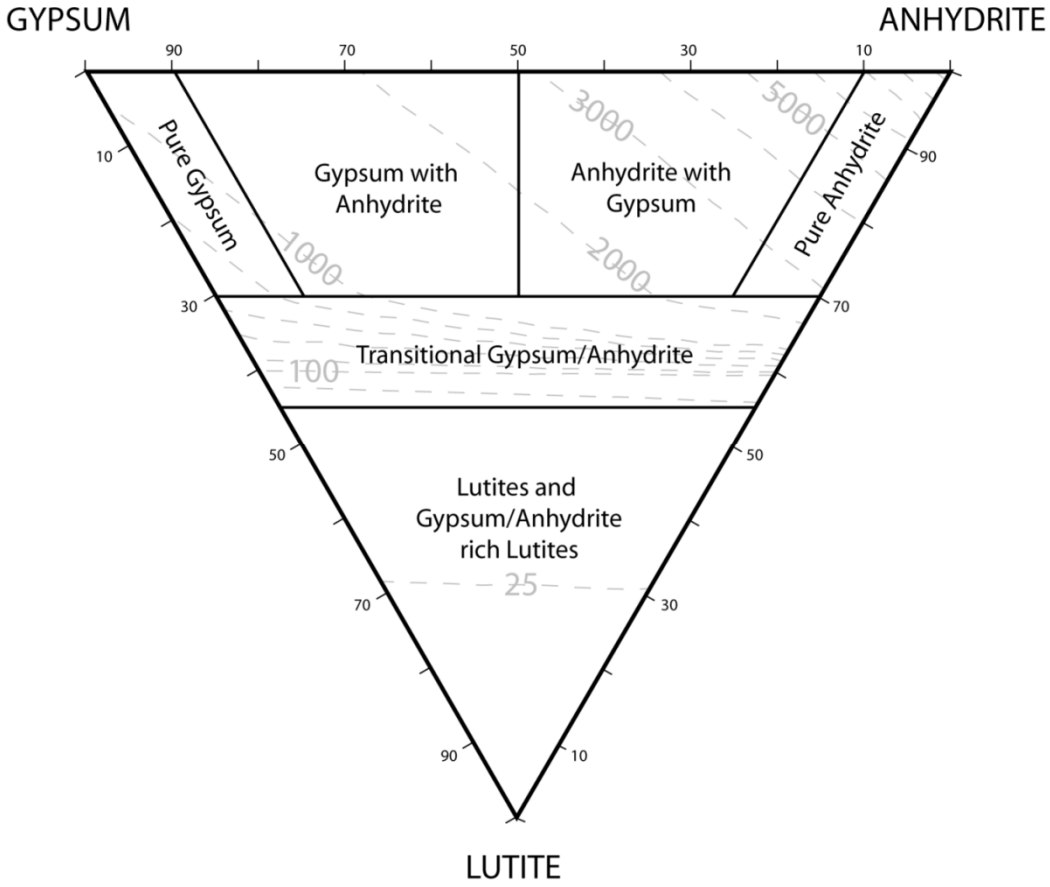
GYPSUM
ANHYDRITE
LUTITE
90
70
50
30
10
Pure Gypsum
Gypsum with Anhydrite
Anhydrite with Gypsum
Pure Anhydrite
3000
5000
1000
2000
Transitional Gypsum/Anhydrite
100
Lutites and Gypsum/Anhydrite rich Lutites
25